Vol. 76: 177–189, 2018
https://doi.org/10.3354/cr01533

CLIMATE RESEARCH
Clim Res

Published online October 10

Leading interannual variability modes of East Asian winter precipitation in CMIP5 general circulation models

Chenxi Jin[1], Yang Yang[2,*], Wenli Guo[1]

[1]Beijing Meteorological Service Center, Beijing 100089, PR China
[2]Institute of Urban Meteorology, China Meteorological Administration, Beijing 100089, PR China

ABSTRACT: This study examined the performances of 19 atmospheric general circulation models, which participated in Coupled Model Intercomparison Project 5 (CMIP5), while simulating East Asian winter (JFM) precipitation. The first 3 leading interannual variability modes of East Asian winter precipitation were obtained using the empirical orthogonal function (EOF) method. Results indicated that the observed first EOF mode, which accounted for 59% of the total variance and is ENSO related, represented a positive precipitation center over southern China. Specifically, the warm sea surface temperature (SST) in the equatorial central eastern Pacific induces an anomalous Philippine Sea anticyclone, and the increased southwesterly winds further transport anomalous water vapor to southern China, which causes more precipitation. EOF1 was well reproduced in the multimodel ensemble mean (MME), with a pattern correlation coefficient (PCC) of 0.84 and a temporal correlation coefficient (TCC) of 0.61. The observed EOF2 exhibited a north–south seesaw pattern, which may be forced by both the western Indian Ocean SST and the high-latitude wave train. The MME partially captured its spatial pattern (with a PCC of 0.48); however, it failed to reproduce its temporal variation (with a TCC of 0.17). The observed EOF3 exhibited an east–west dipole pattern, which was an Arctic Oscillation (AO)-related mode. In the negative AO phase, the strengthened East Asian trough at 500 hPa and the anomalous northerlies were observed to suppress precipitation over East Asia. However, almost all the models, including the MME, poorly simulated the temporal variation of EOF3 because the AO was considered to be an internal mode of the atmosphere.

KEY WORDS: CMIP5 · Winter precipitation · Interannual · Leading modes · ENSO · AO

1. INTRODUCTION

As the East Asian winter monsoon (EAWM) prevails, precipitation in East Asia displays a large interannual variability and can have drastic social and economic effects. Anomalous winter precipitation can have significant effects on agriculture, particularly spring growth. For example, the extremely severe drought that occurred during the winter of 2008–2009 in northern China affected 10 million ha of crops (Gao & Yang 2009). Additionally, heavy winter precipitation may be accompanied by cold air intrusions and may result in freezing rains and snowstorms (Wen et al. 2009, Yu et al. 2015). For instance, a prolonged period of freezing rain and heavy snow hit central and southern China in January 2008, resulting in a substantial amount of economic damage (Ding et al. 2008, Zhou et al. 2011). Therefore, improving the understanding of winter precipitation variations and associated physical mechanisms in East Asia is critical because of the potential climatic, economic and social effects.

However, East Asian winter precipitation has not been given significant attention in previous studies because the frequencies and amounts of winter precipitation are considerably lower than those observed

*Corresponding author: yyang@ium.cn

during other seasons (Li & Ma 2012; see Fig. 1c) and because winter precipitation is primarily concentrated in southern China (Wang & Feng 2011; see Fig. 1a). Previous studies have concentrated on the impact of various factors on East Asian winter precipitation. For instance, a significant positive correlation can be observed between El Niño-Southern Oscillation (ENSO) and winter precipitation in southeastern China from several previous studies (Zhang & Sumi 2002, Wu et al. 2003, Li & Ma 2012, Zhang et al. 2018). During El Niño years, anomalous anticyclones develop over the western North Pacific, and anomalous lower-level southwesterly winds carry water vapor from the Bay of Bengal and the South China Sea (SCS), which favor abnormally heavy winter precipitation in southern China (Feng et al. 2010, Zhou et al. 2010, Lu et al. 2017). Furthermore, East Asian winter precipitation is closely related to the EAWM. During weak EAWM years, southwesterly anomalies that are observed at 700 hPa prevail over the SCS, which results in the transportation of a considerable amount of moisture to southeastern China. Simultaneously, the East Asian westerly jet weakens and displaces southward, contributing to an increase in ascending motion over southeastern China (Zhou & Wu 2010, Zhou 2011). In addition, sea surface temperature (SST) anomalies over the SCS (Zhou et al. 2010, Li et al. 2012), Indian Ocean (Peng 2012, Ren et al. 2017) and north Pacific Ocean (Zhang & Guan 2017), and the Arctic Oscillation (AO) (Mao et al. 2011, Lou et al. 2017) are also considered to be potential modulators of East Asian winter precipitation. Based on observed precipitation data, Wang & Feng (2011) further investigated the first leading modes of winter precipitation and revealed that the leading empirical orthogonal function (EOF) mode of winter precipitation was closely associated with ENSO and the EAWM, whereas EOF2 was related to the barotropic wave train across the Eurasian continent; further, EOF1 and EOF2 accounted for 49.4 and 17.2%, respectively, of the total variance.

Numerical climate models can be used as an essential tool to understand past, present and future climate changes. Coupled Model Intercomparison Project 5 (CMIP5) provides a new platform to investigate the physical mechanisms of climate change and predictability (Rao et al. 2015, Yang et al. 2015). Various studies of winter precipitation simulation have focused on assessing the ability of climate models to simulate the distribution of mean precipitation (Wei et al. 2014) and its interannual standard deviation (Jiang & Tian 2013, Jiang et al. 2016). The precipitations simulated in 34 CMIP5 models are evaluated with respect to observations over 8 regions which exhibit large overall winter precipitation biases in the monsoonal southern China region (Liu et al. 2014). Chen & Frauenfeld (2014) evaluated historical precipitation variability based on 20 CMIP5 models and reported that CMIP5 models could effectively reproduce the spatial pattern of annual and seasonal precipitation over China. Jiang et al. (2016) analyzed 47 CMIP5 models and showed that the majority of the CMIP5 models overestimated the magnitude and spatial variability of the interannual variability of precipitation over China.

However, very few studies have been conducted to evaluate the physical mechanisms and origins of the interannual variations in winter precipitation over East Asia in CMIP5 models, and the majority of the studies that have been conducted mainly focus on the modulation by ENSO (Gong et al. 2014, Jin & Zhou 2014). Gong et al. (2015) indicated that the close ENSO–EAWM relationship exhibits significant impacts on East Asian winter precipitation by 36 CMIP5 models. Lu et al. (2017) investigated the seasonal prediction skill of winter precipitation over southern China using 3 models and indicated that the ENSO and the Indian Ocean are sources of prediction for southern China winter precipitation. However, investigations of the separated and individual physical mechanisms of the leading modes of East Asia precipitation are limited. A comprehensive assessment of the leading interannual modes of winter precipitation variability in CMIP5 models is still lacking. The objective of the present study is to assess the performance of CMIP5 atmospheric general circulation models (GCMs) while simulating the leading interannual variability modes of East Asian winter precipitation, and to verify the potential origins and mechanisms of East Asian winter precipitation.

2. MODELS, DATA AND ANALYSIS METHODS

A total of 19 GCMs, which were driven by monthly historical SST and sea ice and derived from the CMIP5 multimodel dataset, were used in this study. All the data were regridded to 2.5° × 2.5° by bilinear interpolation and were linearly detrended. The model number, model name, horizontal resolution and institutes of the analyzed GCMs are presented in Table 1. In this study, we focused on evaluating monthly model outputs based on the historical run for the period 1979–2008. To focus on interannual variability, we filtered out variations of >8 yr from the original datasets using Lanczos filtering.

The verification datasets included (1) Global Precipitation Climatology Project (GPCP) data (Adler et al.

Table 1. Names, horizontal resolutions and institutes of the 19 CMIP5 atmospheric general circulation models used in this study

No.	Model name	Horizontal resolution	Institute(s)
1	ACCESS1-0	1.3° × 1.9°	Commonwealth Scientific and Industrial Research Organization and Bureau of Meteorology, Australia
2	BCC-CSM1-1	2.8° × 2.8°	Beijing Climate Center, PR China
3	BNU-ESM	2.8° × 2.8°	Beijing Normal University, PR China
4	CanAM4	2.8° × 2.8°	Canadian Centre for Climate Modeling and Analysis, Canada
5	CCSM4	0.9° × 1.3°	NCAR, USA
6	CMCC-CM	0.9° × 1.3°	NCAR, USA
7	CNRM-CM5	1.4° × 1.4°	Centre National de Recherches Météorologiques and Centre Européen de Recherches et de Formation Avancée en Calcul Scientifique, France
8	FGOALS-g2	3° × 2.8°	Institute of Atmospheric Physics (IAP) and Tsinghua University, PR China
9	FGOALS-s2	1.7° × 2.8°	IAP, PR China
10	GISS-E2-R	2.0° × 2.5°	NASA Goddard Institute for Space Studies, USA
11	HadGEM2-A	1.3° × 1.9°	Met Office Hadley Center, UK
12	INMCM4	1.5° × 2°	Institute for Numerical Mathematics, Russia
13	IPSL-CM5A-LR	1.9° × 3.8°	Institut Pierre Simon Laplace, France
14	MIROC5	1.4° × 1.4°	Atmosphere and Ocean Research Institute, National Institute for Environmental Studies, and Japan Agency for Marine-Earth Science and Technology, Japan
15	MPI-ESM-LR	1.9° × 1.9°	Max Planck Institute for Meteorology (MPI-M), Germany
16	MPI-ESM-MR	1.9° × 1.9°	MPI-M, Germany
17	MRI-AGCM3-2H	0.6° × 0.6°	Meteorological Research Institute (MRI), Japan
18	MRI-AGCM3-2S	0.2° × 0.2°	MRI, Japan
19	NorESM1-M	1.9° × 2.5°	Norwegian Climate Centre, Norway

2003), (2) NCEP–DOE AMIP II reanalysis (NCEP2) data (Kanamitsu et al. 2002) and (3) SST data derived from NOAA extended reconstructed SST version 3b (ERSSTV3b) data (Smith et al. 2008). Additionally, we used the monthly Niño 3.4 and AO indices from NOAA's Climate Prediction Center website (www.cpc.ncep.noaa.gov/).

Previous studies have found that there is a significant positive correlation between ENSO and South China precipitation during January–March (JFM) rather than during the traditional December–February (DJF) winter months (Zeng et al. 2010, Zhou et al. 2010). Therefore, we focused on winter precipitation in JFM, which was slightly different from the traditional DJF mean.

3. RESULTS

3.1. Climatology of East Asian winter precipitation based on observation and GCMs

A comparison of climatological winter (JFM) precipitation between the GPCP and CMIP5 multimodel ensemble mean (MME) is depicted in Fig. 1. In the following model evaluations, the GPCP refers to observational metrics (i.e. the observation). In the observations, the subtropical precipitation band extended from southeastern China to Japan due to sufficient water vapor transportation from the SCS and the Bay of Bengal by southwesterly winds (Fig. 1a). The percentage of annual total precipitation in winter reaches 20% over southeastern China (Fig. 1c). These features are reasonably reproduced by the MME (Fig. 1b,d), with a pattern correlation coefficient (PCC) of 0.89, which is statistically significant at the 5% level.

To objectively measure the ability of the 19 GCMs in simulating the climatology of winter precipitation over East Asia, the PCCs, standard deviation and centered root mean square difference (RMSD) between the simulated and observed climatology precipitation data in winter from 1979 to 2008 were evaluated. As exhibited in the Taylor diagram (Taylor 2001), all 19 GCMs reliably reproduced the distribution of winter precipitation (Fig. 2), with the PCCs ranging from 0.36 (BNU-ESM) to 0.90 (MRI-AGCM3-2H), and were statistically significant at the 5% level using 2-tailed 1-sample *t*-tests. The normalized centered RMSDs ranged from 0.62 (INMCM4) to 1.2 (BNU-ESM and GISS-E2-R). Because the MME eliminated model un-

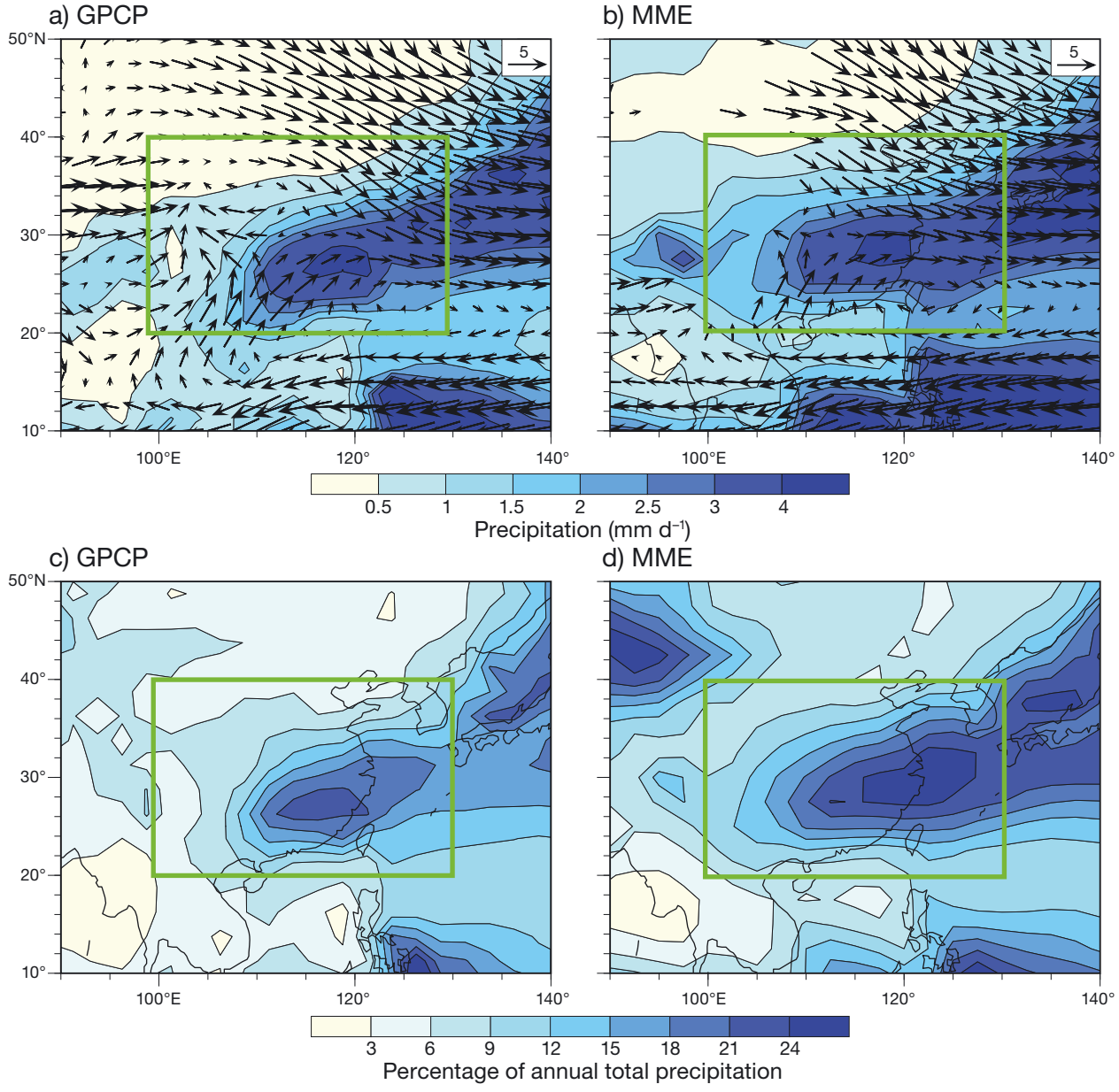

Fig. 1. (a) Climatological winter (JFM) precipitation (shaded) and winds at 850 hPa (vector, m s^{-1}; scale arrows top-right in panels) for the period from 1979 to 2008; (b) percentage of annual total precipitation in JFM. (a,c) Global Precipitation Climatology Project (GPCP) and (b,d) multimodel ensemble mean (MME)

certainty, the description of the spatial distribution in the MME was more accurate than that in an individual model, with a PCC (RMSD) of 0.88 (0.54).

3.2. Leading modes of East Asian winter precipitation

The first 4 leading EOF modes were well distinguished from each other in both the observation and the simulation (not shown), as demonstrated by North et al. (1982). In this section, the first 3 leading modes of winter precipitation variability over the East Asian region (20°–40° N, 100°–130° E) were investigated using observation and simulation using GCMs.

As depicted in Fig. 3a, the observed first leading mode represented the strength of precipitation over southern China and accounted for 59% of the total variance. The spatial pattern in the MME (Fig. 3g) resembled the observation reasonably well and accounted for 60.5% of the total variance. The PCC between the observation and the MME was 0.84 and was statistically significant at the 5% level. The temporal variation of the first leading mode was also sim-

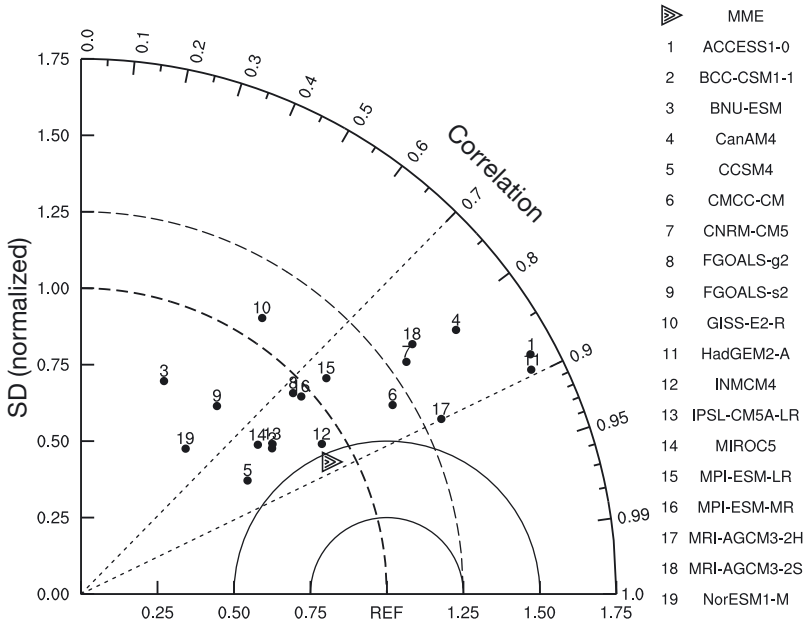

Fig. 2. Taylor diagram displaying the pattern statistics of climatological winter precipitation from 1979 to 2008. The abscissa (ordinate) represents the correlation coefficients (standard deviation, SD) between the observed and simulated JFM precipitation over the East Asian region (20°–40° N, 100°–130° E). The arrowhead represents the results of the multi-model ensemble mean (MME). The nearer the distance between a number and the reference (REF), the better will be the performance of the corresponding model

ulated reasonably well in the MME (Fig. 3d,j). The temporal correlation coefficient (TCC) between the first principal component (PC1) of the observation and that of the MME is 0.61. Because the MME suppresses the internal variability of the atmosphere and reflects the signals of SST anomalies, the high PCC (0.84) and TCC (0.61) between the first leading mode of the observation and that of the MME, which are statistically significant at the 5% level, indicate that the first leading mode of East Asian winter precipitation, which accounts for 60% of the total variance, is highly reproducible once the SST anomalies are prescribed.

The spatial pattern of the second observed mode (Fig. 3b), which explained 16.3% of the total variance, exhibited a north–south seesaw pattern with negative anomalies over the south at 25° N and positive anomalies over southeastern China. The MME reproduced the seesaw pattern reasonably well, with a slightly higher percentage of the total variance (20.3%) as compared to the observed value (Fig. 3h). However, the simulated center position shifts further southward (Fig. 3h vs. Fig. 3b). The PCC between the second mode of the observation and that of the MME is 0.48, which is statistically significant at the 5% level.

The spatial pattern of the third mode of observational precipitation, which accounts for 9.7% of the total variance, is exhibited in Fig. 3c. This mode depicted an east–west dipole pattern in the target area, with positive center anomalies located around 27° N and 120° E and with negative anomalies located to the west of 115° E. The MME partially captured its spatial pattern (Fig. 3i), with 5.6% of the total variance. The PCC between the third mode of the observation and that of the MME was 0.64 and was statistically significant at the 5% level.

The temporal variations shown in Fig. 3e (PC2) and Fig. 3f (PC3) for the observation respectively, and those in Fig. 3k (PC2) and Fig. 3l (PC3) for the MME, indicate significant interannual variability. However, the TCCs between the observation and the MME for PC2 (0.17) and PC3 (0.10) were not significant. It should be noted that the low TCCs in PC2 and PC3 do not represent the poor ability of the CMIP5 GCMs; instead, they reflect that the second and third leading modes may not be forced by SST.

The performance of 19 GCMs simulating the first 3 leading modes of East Asian winter precipitation are presented in Fig. 4. The PCC and TCC are used to assess the skills of both the spatial patterns and PCs for the first 3 leading modes. To avoid a possible mismatch between the order of EOF in the model and that in the observation, we initially calculated the PCC for each EOF mode between the models and that in the observation and further selected the EOF modes according to the highest PCC with respect to the observation as the corresponding EOF modes in the models. The skill of the first leading mode is represented in Fig. 4a. The PCCs between the observation and most models were higher than 0.5, which was statistically significant at the 5% level, indicating that the majority of the models can reproduce the spatial pattern of the first leading mode. However, among the 19 models, only 8 models (ACCESS1-0, BNU-ESM, CCSM4, FGOALS-s2, GISS-E2-R, Had GEM2-A, MPI-ESM-LR and MRI-AGCM3-2S) exhibited that the TCCs of PC1 between the observation and the simulation were statistically significant at the 5% level.

The performances of the GCMs in deriving the second (Fig. 4b) and third (Fig. 4c) leading modes were

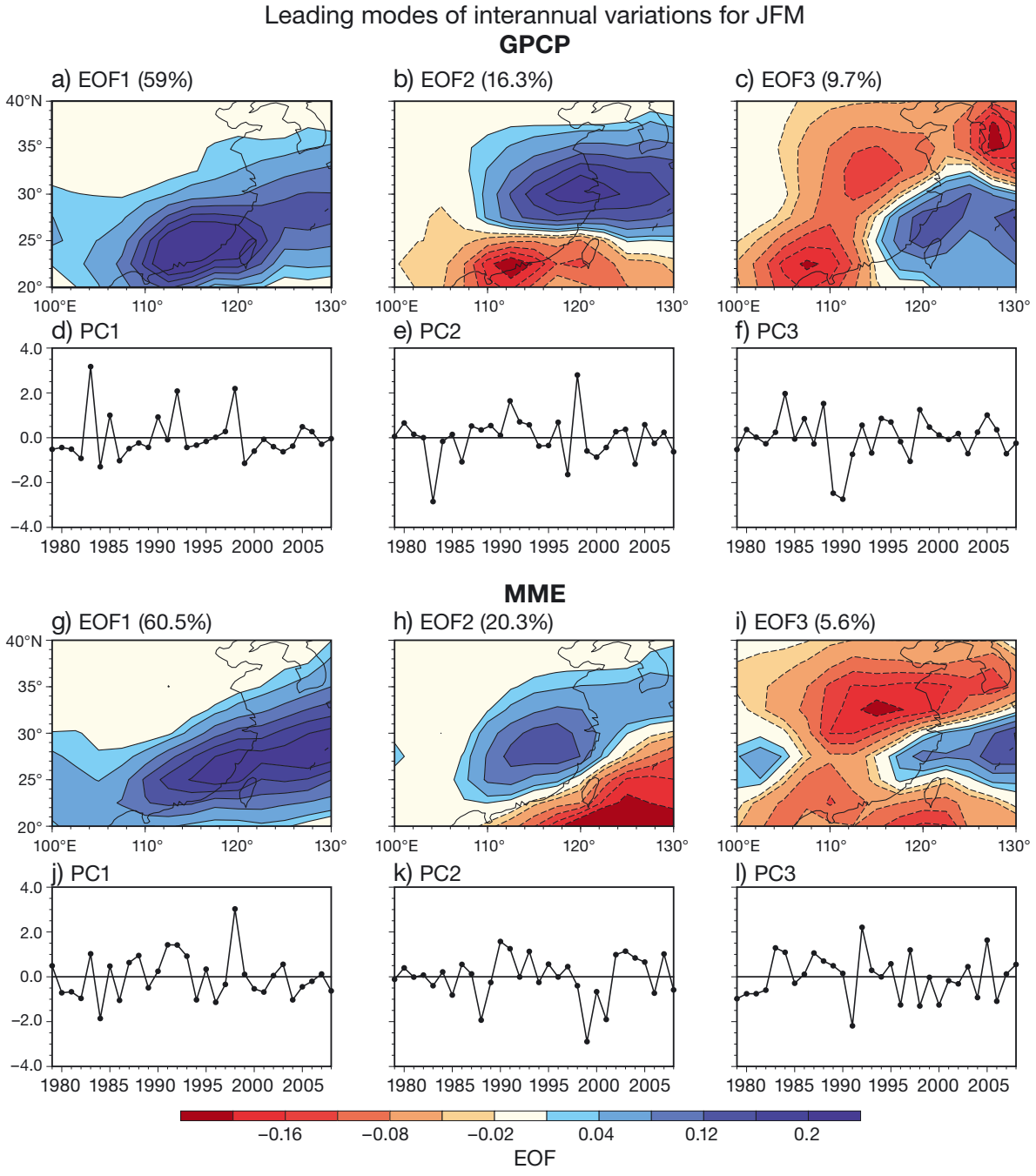

Fig. 3. Comparison of the first 3 leading modes of the (a–f) Global Precipitation Climatology Project (GPCP) and (g–l) multimodel ensemble mean (MME) precipitation anomalies over the East Asian domain (20°–40° N, 100°–130° E) derived for January–March, 1979–2008. The fractional variance for each mode is also depicted. PC: principal component

generally worse than those in deriving the first leading mode. The majority of the models reproduced the spatial pattern reasonably well, especially IPSL-CM5A-LR and CCSM4, which are recommended for conducting research on the EAWM. However, almost all the models performed poorly in terms of temporal variations in PC2 and PC3.

3.3. Origins of the leading modes of East Asian winter precipitation

The origins of the leading modes of winter precipitation are analyzed in this section. Fig. 5 presents the lead–lag correlation coefficients between the equatorial Indo-Pacific SST anomalies averaged over 10° S–

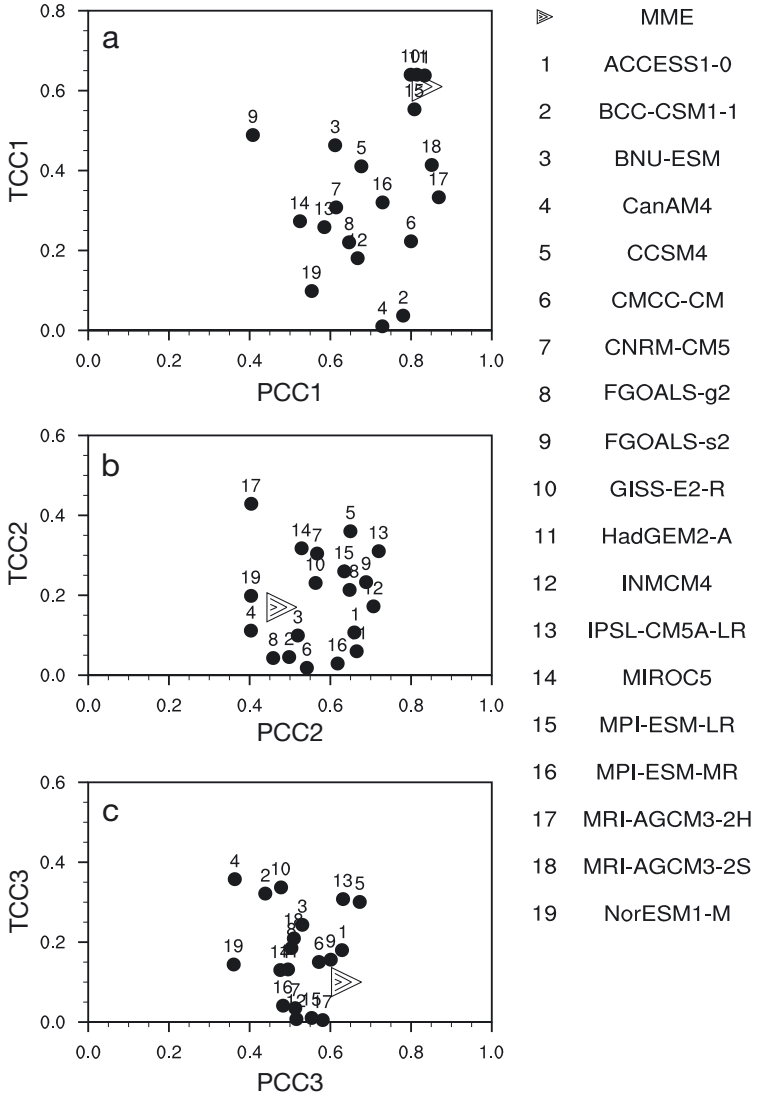

Fig. 4. Performances of the simulated (a) first leading mode, (b) second leading mode and (c) third leading mode. The abscissa (ordinate) represents the pattern (time) correlation coefficient between the observed and simulated anomalies. The arrowhead represents the results of the multi-model ensemble mean (MME). TCC: temporal correlation coefficient; PCC: pattern correlation coefficient

10° N and the PCs in observations (Fig. 5a,c,e) and the MME (Fig. 5b,d,f). As depicted in Fig. 5a, the observed first leading mode exhibits a significant positive (negative) lead correlation with the equatorial eastern (western) Pacific SST anomalies and a positive simultaneous correlation with the eastern Indian SST anomalies. Furthermore, the TCC between the observed PC1 and Niño 3.4 index is 0.57, which is statistically significant at the 5% level. Therefore, the first leading mode may be forced by ENSO, which is also indicated in a previous study based on observational data (Wang & Feng 2011). Meanwhile, the lead–lag correlation of SST and PC1 in the MME displayed features similar to those in the observations (Fig. 5b vs. Fig. 5a), and the TCC between PC1 in the MME and the Niño 3.4 index (0.62) was comparable to that in the observations, indicating that the first leading mode in the MME was also forced by ENSO and that the ENSO-related first leading mode was reproduced reasonably well in the MME (Fig. 5b).

The observed second leading mode is positively correlated with the equatorial western Indian Ocean SST anomalies (Fig. 5c). However, the significant SST anomalies of the simulated second mode were located at the equatorial central and western Pacific, which resembled the pattern of El Niño in the central Pacific Ocean (Fig. 5d). The third mode had no significant relationship with the equatorial Indo-Pacific SST anomalies in both the observation and the MME simulation (Fig. 5e,f).

To investigate the pattern in the first leading mode, precipitation and wind at 850 hPa are regressed on the observed PC1 (Fig. 6a). The anomalous anticyclone in the Philippine Sea was the key factor that transported water vapor from the ocean to southern China through increased southwesterly winds (Wang & Zhang 2002). In response to El Niño, induced warm SST anomalies prevailed over the equatorial central eastern Pacific and cold SST anomalies prevailed over the western North Pacific (Fig. 6e), and the anomalous anticyclone in the Philippine Sea was formed due to enhanced wind–evaporation/entrainment–SST feedback (Wang et al. 2000). Additionally, the upper troposphere was characterized by a dipole pattern with a convergence center in the Philippine Sea and a divergence center over the equatorial eastern Pacific (Fig. 6c). The MME reproduced these atmospheric circulations reasonably well (Fig. 6b,d,f).

As depicted in Fig. 5b, the observed second mode may be associated with the equatorial western Indian Ocean SST anomalies. The corresponding atmospheric circulation pattern is exhibited in Fig. 7. The anomalous upward motions over the western Indian Ocean caused by the local warm SST led to a divergence center that was located above the western Indian Ocean (Fig. 7c). Correspondingly, the upper

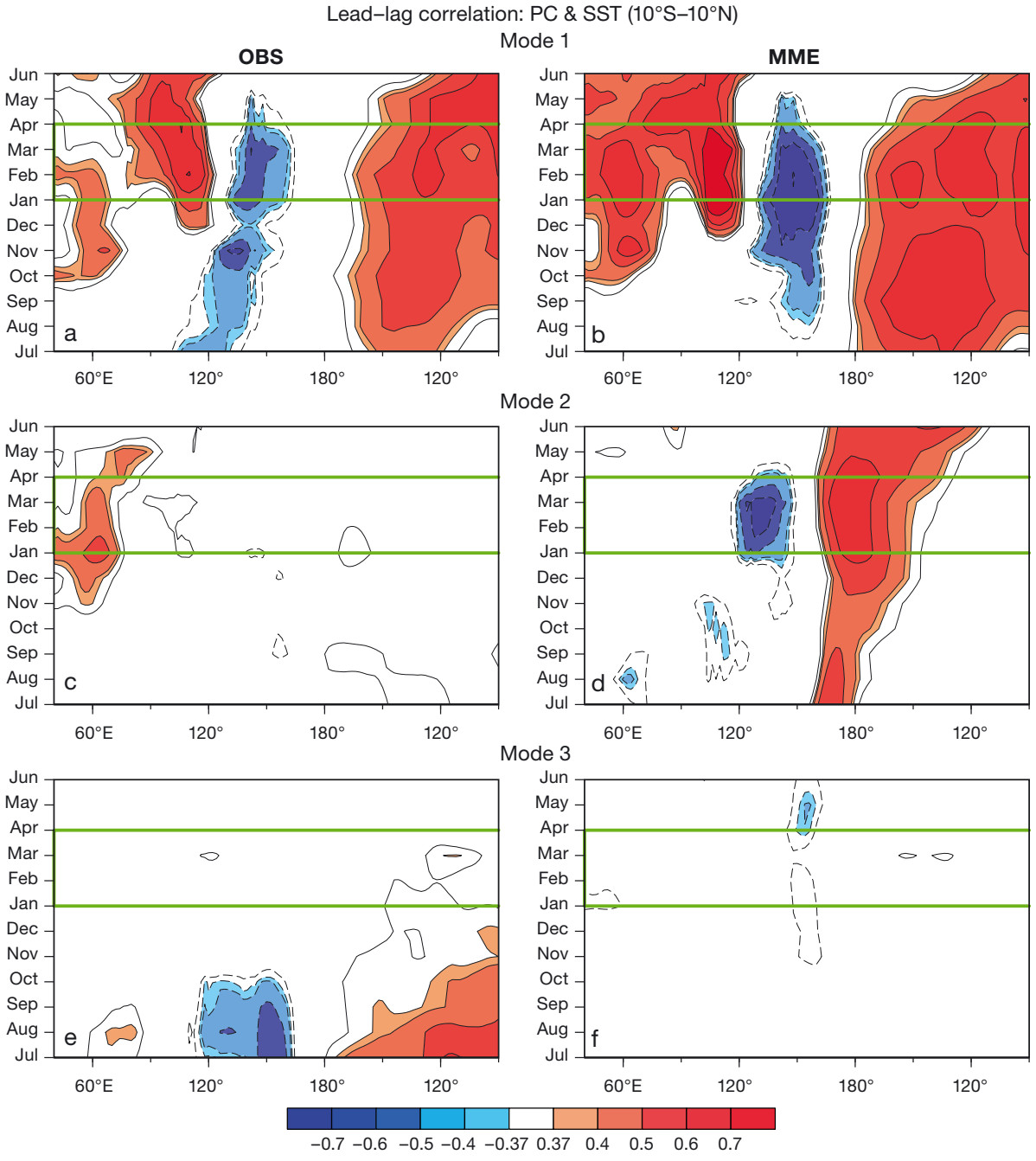

Fig. 5. Relationship between the principal components (PCs) and the equatorial Indian–Pacific (40° E–90° W) SST anomalies averaged between 10° S and 10° N. The relationships are exhibited by the lead–lag correlation coefficients of SST anomalies with reference to (a) PC1, (c) PC2 and (e) PC3 of the observations (OBS); (b,d,f) are same as (a,c,e) but for those of the multimodel ensemble mean (MME). The shading denotes the areas at which the correlation coefficient is statistically significant at the 5% level. Green boxes indicate the January–March period

level convergence center is in the Philippine Sea (Fig. 7c), which induces a low-level anticyclone (Fig. 7a). Thus, the anomalous southwesterly winds transport water vapor from the SCS to eastern China, causing a dipole pattern with positive precipitation in eastern China and with negative precipitation in southern China (Fig. 7a). Fig. 7e exhibits the significantly negative temperature anomalies in Siberia, indicating the influence of the oscillation from high latitude, which is exhibited as a barotropic wave train across the Eurasian continent (Wang & Feng 2011). Thus, the observed second mode was associated with

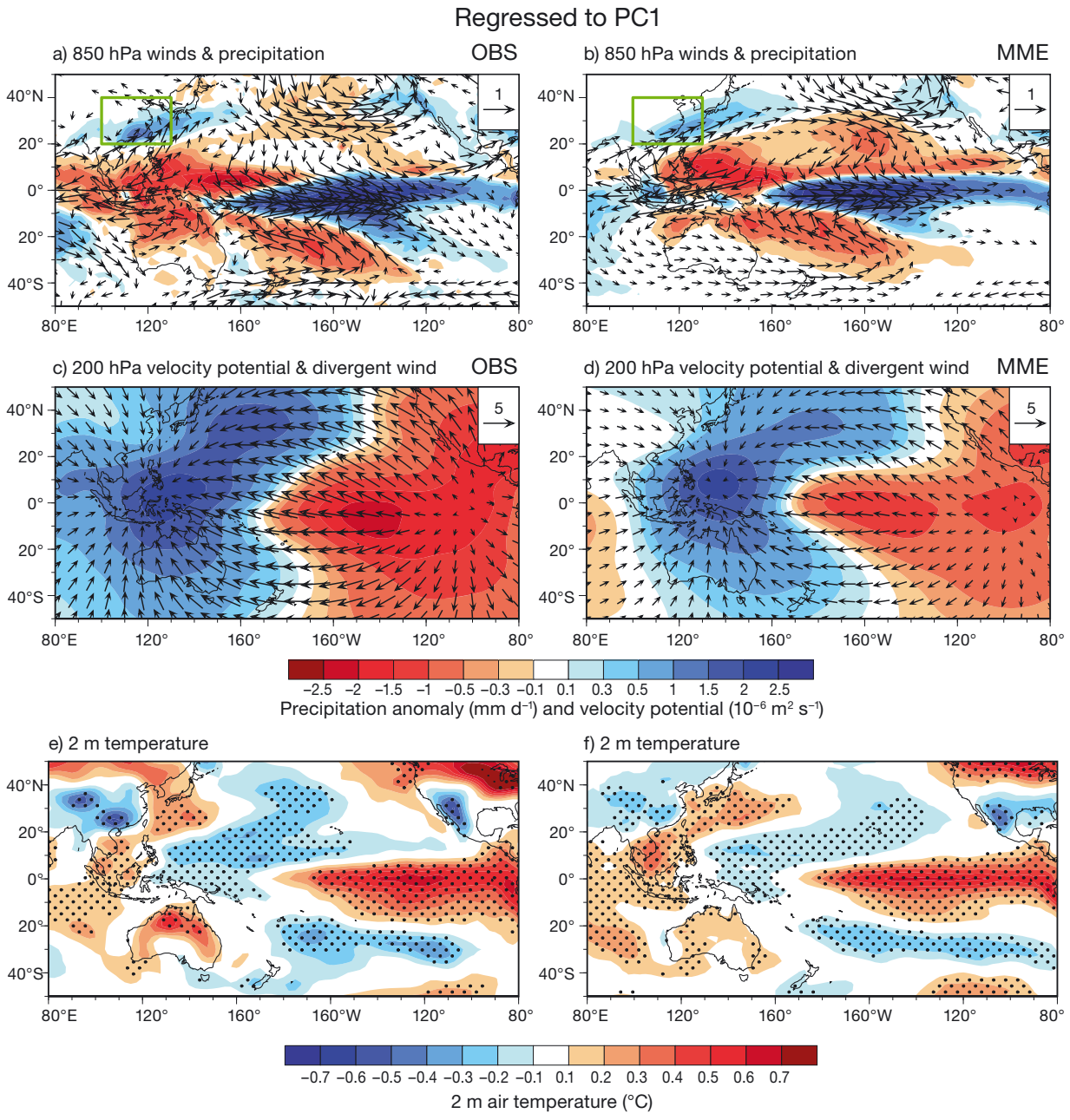

Fig. 6. Wind anomalies at 850 hPa (vector, m s^{-1}, scale arrows top-right in panels), precipitation anomalies (shaded), velocity potential at 200 hPa (shaded), divergent wind (vector, m s^{-1}) and 2 m air temperature (shaded) regressed on principal component 1 (PC1) in (a,c,e) of the observations (OBS); (b,d,f) are same as (a,c,e) but for the multimodel ensemble mean (MME). The dotted regions indicate the areas at which the regression coefficient is statistically significant at the 5% level. The East Asian domains used to perform the EOF analysis are outlined by the green boxes in (a,b)

both the equatorial western Indian Ocean SST and the high-latitude wave train. The surface anticyclone at low latitude can be reproduced by the MME (Fig. 7b). However, it was induced by warm SST anomalies over the central equatorial Pacific Ocean (Fig. 7f), with a divergence center that was located above the central equatorial Pacific (Fig. 7d). Additionally, the MME failed to reproduce the observed temperature anomalies over East Asia (Fig. 7f), indicating that the high-latitude atmospheric circulation variability may be independent of the SST.

To explore the origin of the third leading mode, the circulations in high and low levels are regressed on the observed PC3 (Fig. 8). The strengthened East Asian trough at 500 hPa (Fig. 8a) and enhanced gradient of the west–east sea level pressure anomalies

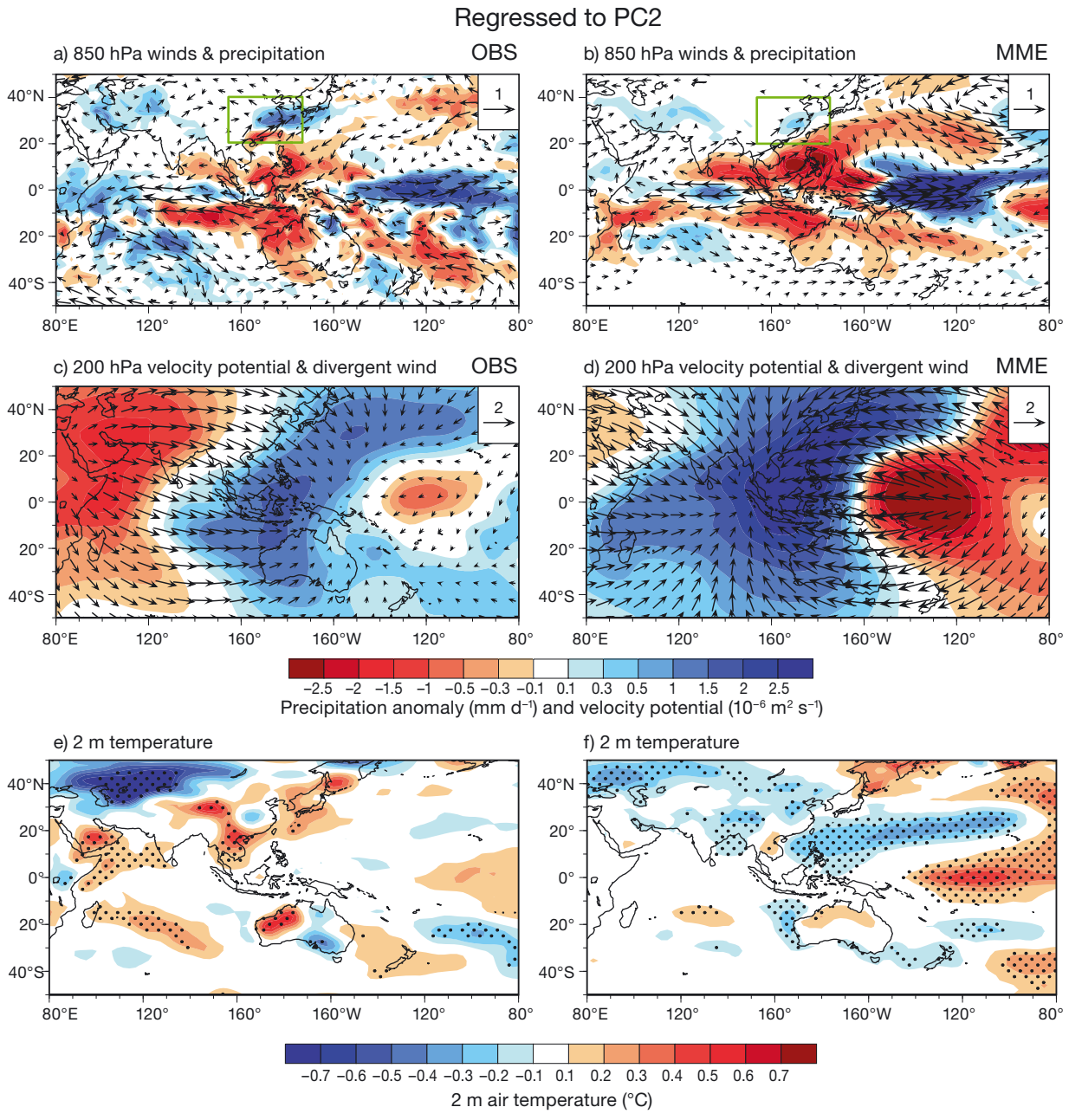

Fig. 7. Same as Fig. 6 but regressed on principal component 2 (PC2)

between the Siberian High and Aleutian Low (Fig. 8c), which were similar to the AO-related circulations, were favorable for inducing the stronger EAWM (Fig. 8c). The anomalous northerlies may lead to cold air temperatures (Fig. 8e) and less precipitation (Fig. 8a) in the East Asian region. Because the TCC between the observed PC3 and the AO index was –0.59, the third leading mode may be related to the AO. As an internal mode of the atmosphere, the interannual variability of the AO was not significantly influenced by SST (Yamazaki & Shinya 1999). Therefore, the MME failed to reproduce the observed atmospheric circulation pattern of the third leading mode; further, the observed precipitation anomalies were poorly simulated (Fig. 8b,d,f). We additionally verify the relationship between the AO and EOF3 in the individual model, and the results exhibit that some models present a high TCC between PC3 and the AO index, including ACCESS1-0, CCSM4 and MPI-ESM-MR, which can be adopted to further investigate the impact of the AO on the third mode of winter precipitation.

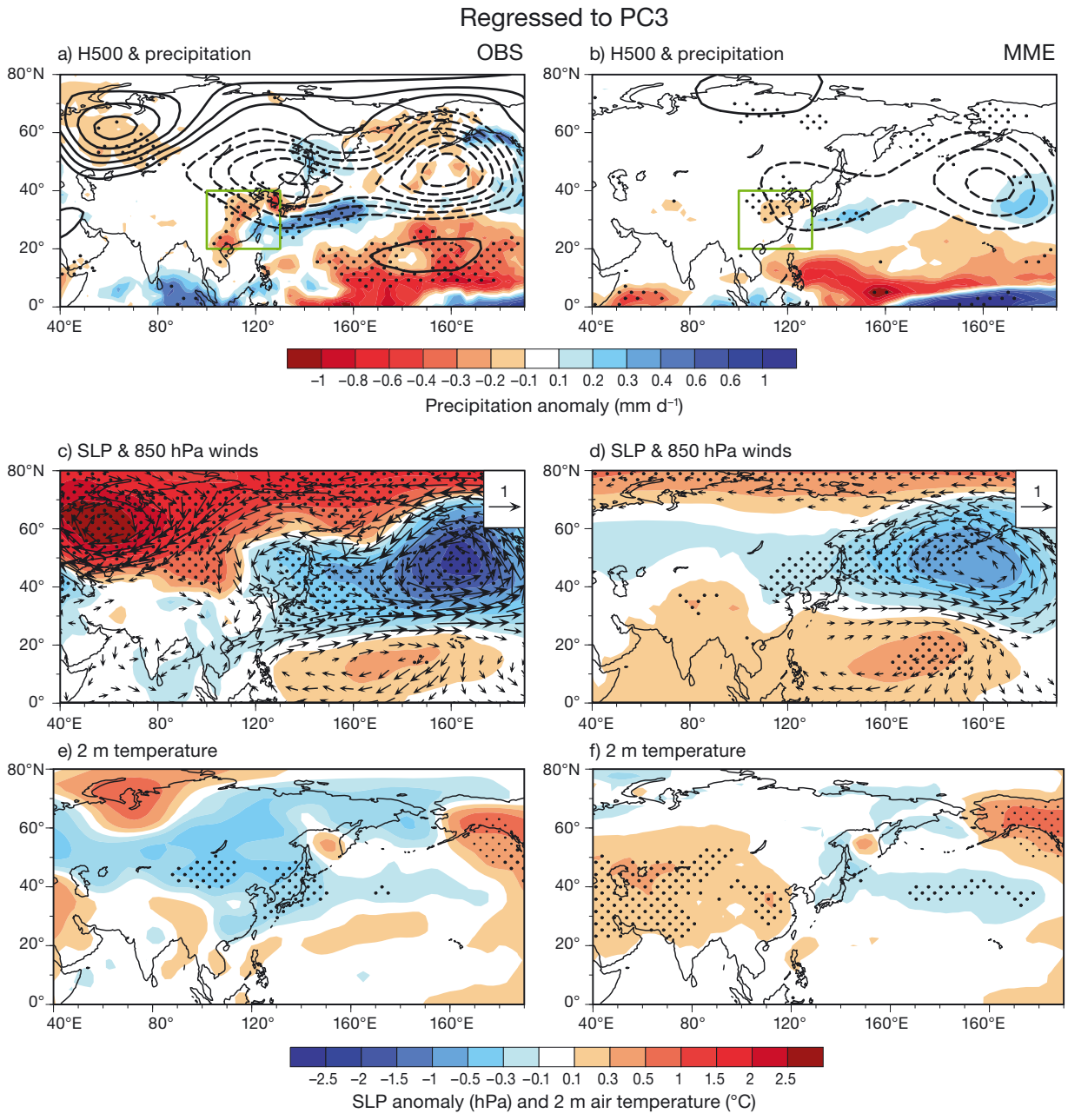

Fig. 8. Geopotential height anomalies at 500 hPa (H500) (contour, gpm), precipitation anomalies (shaded), sea level pressure anomalies (SLP) (shaded), wind anomalies at 850 hPa (vector, m s^{-1}, scale arrows top-right in panels) and 2 m air temperature (shaded) regressed on principal component 3 (PC3) in (a,c,e) of the observations; (b,d,f) are same as (a,c,e) but for the multi-model ensemble mean (MME). The dotted regions indicate the areas in which the regression coefficient is statistically significant at the 5% level. The East Asian domains used to perform the EOF analysis are outlined by the green boxes in (a,b)

4. SUMMARY AND DISCUSSION

The leading interannual variability modes of winter precipitation over East Asia were investigated by analyzing the outputs of 19 CMIP5 GCMs which were forced by prescribed historical SST and sea ice. The major findings and results can be summarized as follows:

1. The observed climatological distribution of winter precipitation was well reproduced by the majority of the CMIP5 GCMs. The performance of the MME was better than that of each model.

2. The observed first leading mode accounted for 59% of the total variance and represented the positive precipitation center in southern China. The MME accurately reproduced the spatial and tempo-

ral variation of the first leading mode, with PCC and TCC values of 0.84 and 0.61, respectively, and a total variance (60.5%) comparable to the observation. Further analysis indicated that the first leading mode was an ENSO-related mode, which can be well simulated in GCMs forced by historical SST.

3. The observed second leading mode exhibited a north–south seesaw pattern that may be associated with both the western Indian Ocean SST and the high-latitude wave train. The MME can partially reproduce the spatial pattern, including the surface anticyclone at low latitude, which was induced by warm SST anomalies over the central equatorial Pacific Ocean. However, the MME failed to simulate the temporal variability because the high-latitude atmospheric circulation variability may be independent of SST.

4. The observed third leading mode was an AO-related mode, with the TCC between the observed PC3 and the AO index of −0.59. The negative AO phase resulted in the strengthened East Asian trough at 500 hPa and the enhanced gradient of west–east sea level pressure anomalies between the Siberian High and Aleutian Low, which was favorable for the cold air temperature and for less precipitation in the East Asian region. The MME failed to reproduce the observed atmospheric circulation pattern because the AO was considered to be an internal mode of the atmosphere.

Note that the results in the present study were based on the GCMs which were driven by the prescribed SST. The atmospheric origin and the air–sea interaction may play an important role in shaping some EOF modes as well as SST, which requires further analysis by adopting coupled model simulations.

Acknowledgements. We thank the modeling groups who have participated in CMIP5 and the Program for Climate Model Diagnosis and Intercomparison (PCMDI), which provided the model data. This research was jointly supported by the National Natural Science Foundation of China (Grant No. 41705076) and the Beijing Science and Technology Commission (Grant Nos. Z161100001116098 and D171100000717002).

LITERATURE CITED

Adler RF, Huffman GJ, Chang A, Ferraro R and others (2003) The version-2 Global Precipitation Climatology Project (GPCP) monthly precipitation analysis (1979–present). J Hydrometeorol 4:1147–1167

Chen L, Frauenfeld OW (2014) A comprehensive evaluation of precipitation simulations over China based on CMIP5 multimodel ensemble projections. J Geophys Res Atmos 119:5767–5786

Ding YH, Wang ZY, Song YF, Zhang J (2008) Causes of the unprecedented freezing disaster in January 2008 and its possible association with global warming. Acta Meteorol Sin 66:808–825 (in Chinese)

Feng J, Wang L, Chen W, Fong SK, Leong KC (2010) Different impacts of two types of Pacific Ocean warming on southeast Asian rainfall during boreal winter. J Geophys Res 115:D24122

Gao H, Yang S (2009) A severe drought event in northern China in winter 2008–2009 and the possible influences of La Niña and Tibetan Plateau. J Geophys Res 114: D24104

Gong HN, Wang L, Chen W, Wu RG, Wei K, Cui X (2014) The climatology and interannual variability of the East Asian winter monsoon in CMIP5 models. J Clim 27:1659–1678

Gong HN, Wang L, Chen W, Nath D, Huang G, Tao WC (2015) Diverse influences of ENSO on the East Asian–western Pacific winter climate tied to different ENSO properties in CMIP5 models. J Clim 28:2187–2202

Jiang DB, Tian ZP (2013) East Asian monsoon change for the 21th century: results of CMIP3 and CMIP5 models. Chin Sci Bull 58:1427–1435

Jiang DB, Tian ZP, Lang X (2016) Reliability of climate models for China through the IPCC third to fifth assessment reports. Int J Climatol 36:1114–1133

Jin CX, Zhou TJ (2014) Analysis of the interannual variations of the East Asian winter monsoon simulation by four CMIP5 GCMs. Chin J Atmos Sci 38:453–468 (in Chinese)

Kanamitsu M, Ebisuzaki W, Woollen J, Yang SK and others (2002) NCEP–DOE AMIP-II reanalysis (R-2). Bull Am Meteorol Soc 83:1631–1643

Li C, Ma H (2012) Relationship between ENSO and winter rainfall over southeast China and its decadal variability. Adv Atmos Sci 29:1129–1141

Li WB, Feng JX, Chen SM, Wang L (2012) Relationship between wintertime precipitation in South China and air–sea heat fluxes. Atmos Sci Lett 13:113–119

Liu Z, Mehran A, Phillips TJ, AghaKouchak A (2014) Seasonal and regional biases in CMIP5 precipitation simulations. Clim Res 60:35–50

Lou MY, Li C, Hao SF, Liu J (2017) Variations of winter precipitation over southeastern China in association with the North Atlantic Oscillation. J Meteor Res 31:476–489

Lu B, Scaife AA, Dunstone N, Smith D and others (2017) Skillful seasonal predictions of winter precipitation over southern China. Environ Res Lett 12:074021

Mao R, Gong DY, Yang J, Bao JD (2011) Linkage between the Arctic Oscillation and winter extreme precipitation over central-southern China. Clim Res 50:187–201

North GR, Bell TL, Cahalan RF, Moeng FJ (1982) Sampling errors in the estimation of empirical orthogonal functions. Mon Weather Rev 110:699–706

Peng JB (2012) Influence of the sea surface temperature in the eastern Indian Ocean on the wintertime rainfall in the southern part of China. Clim Environ Res 17:327–338 (in Chinese)

Rao J, Ren RC, Yang Y (2015) Parallel comparison of the northern winter stratospheric circulation in reanalysis and in CMIP5 models. Adv Atmos Sci 32:952–966

Ren Q, Zhu ZW, Hao LP, He JH (2017) The enhanced relationship between southern China winter rainfall and warm pool ocean heat content. Int J Climatol 37:409–419

Smith TM, Reynolds RW, Peterson TC, Lawrimore J (2008) Improvements to NOAA's historical merged land–ocean surface temperature analysis (1880–2006). J Clim 21: 2283–2296

Taylor KE (2001) Summarizing multiple aspects of model performance in a single diagram. J Geophys Res 106: 7183–7192

Wang B, Zhang Q (2002) Pacific-East Asian teleconnection. II. How the Philippine Sea anomalous anticyclone is established during El Niño development. J Clim 15: 3252–3265

Wang L, Feng J (2011) Two major modes of the wintertime precipitation over China. Chin J Atmos Sci 35:1105–1116 (in Chinese)

Wang B, Wu RG, Fu XH (2000) Pacific-East Asia teleconnection: How does ENSO affect East Asian climate? J Clim 13:1517–1536

Wei K, Xu T, Du ZC, Gong HN and others (2014) How well do the current state-of-the-art CMIP5 models characterize the climatology of the East Asian winter monsoon? Clim Dyn 43:1241–1255

Wen M, Yang S, Kumar A, Zhang PQ (2009) An analysis of the large-scale climate anomalies associated with the snowstorms affecting China in January 2008. Mon Weather Rev 137:1111–1131

Wu RG, Hu ZZ, Kirtman BP (2003) Evolution of ENSO-related rainfall anomalies in East Asia. J Clim 16: 3741–3757

Yamazaki K, Shinya Y (1999) Analysis of the Arctic Oscillation simulated by AGCM. J Meteorol Soc Jpn 77:1287–1298

Yang Y, Ren RC, Cai M, Rao J (2015) Attributing analysis on the model bias in surface temperature in the climate system model FGOALS-s2 through a process-based decomposition method. Adv Atmos Sci 32:457–469

Yu YY, Ren RC, Cai M (2015) Dynamical linkage between cold air outbreaks and intensity variations of the meridional mass circulation. J Atmos Sci 72:3214–3232

Zeng J, Zhang Q, Wang T (2010) Analysis on relationship of East Asian winter monsoon intensity and winter precipitation in southern China. Plateau Meteorol 29:975–981 (in Chinese)

Zhang Q, Guan Z (2017) Interdecadal change in the Eurasia–Pacific anti-phase relation of atmospheric mass and its possible link with PDO. J Meteor Res 31:126–141

Zhang RH, Sumi A (2002) Moisture circulation over East Asia during El Niño episode in northern winter, spring and autumn. J Meteorol Soc Jpn 80:213–227

Zhang Q, Guan Z, Li M (2018) The Eurasia–North Pacific Oscillation in atmospheric mass variations independent of both IHO and AO and its possible impacts on winter climate. Clim Dyn 50:4303–4322

Zhou LT (2011) Impact of East Asian winter monsoon on rainfall over southeastern China and its dynamical process. Int J Climatol 31:677–686

Zhou LT, Wu RG (2010) Respective impacts of East Asian winter monsoon and ENSO on winter rainfall in China. J Geophys Res 115:D02107

Zhou LT, Tam CY, Zhou W, Chan JCL (2010) Influence of South China Sea SST and the ENSO on winter rainfall over South China. Adv Atmos Sci 27:832–844

Zhou BZ, Gu LH, Ding YH and others (2011) The great 2008 Chinese ice storm: its socioeconomic–ecological impact and sustainability lessons learned. Bull Am Meteorol Soc 92:47–60

Editorial responsibility: Guoyu Ren, Beijing, China

Submitted: February 14, 2018; Accepted: August 16, 2018
Proofs received from author(s): October 2, 2018